01 Oct 2020

Microstructural Influence on Mechanical Properties of a Lightweight Ultrahigh Strength Fe-18Mn-10Al-0.9C-5Ni (wt%) Steel

Michael Piston

Laura Bartlett
Missouri University of Science and Technology, lnmkvf@mst.edu

Krista R. Limmer

Daniel M. Field

Recommended Citation

M. Piston et al., "Microstructural Influence on Mechanical Properties of a Lightweight Ultrahigh Strength Fe-18Mn-10Al-0.9C-5Ni (wt%) Steel," *Metals*, vol. 10, no. 10, pp. 1-14, MDPI, Oct 2020.

metals

MDPI

Article

Microstructural Influence on Mechanical Properties of a Lightweight Ultrahigh Strength Fe-18Mn-10Al-0.9C-5Ni (wt%) Steel

Michael Piston [1], Laura Bartlett [1,*], Krista R. Limmer [2] and Daniel M. Field [2]

[1] Materials Science and Engineering Department, Missouri University of Science and Technology, Rolla, MO 65409, USA; mpbdb@mst.edu

[2] Weapons and Materials Research Directorate, US Army Combat Capabilities Development Command Army Research Laboratory, Aberdeen Proving Ground, MD 21005, USA; krista.r.limmer.civ@mail.mil (K.R.L.); daniel.m.field6.civ@mail.mil (D.M.F.)

* Correspondence: lnmkvf@umsystem.edu; Tel.: +1-573-341-4972

Received: 5 August 2020; Accepted: 25 September 2020; Published: 29 September 2020

Abstract: This study evaluates the role of thermomechanical processing and heat treatment on the microstructure and mechanical properties of a hot rolled, annealed, and aged Fe-18Mn-10Al-0.9C-5Ni (wt%) steel. The steel exhibited rapid age hardening kinetics when aged in the temperature range of 500–600 °C for up to 50 h, which has been shown in other work to be the result of B2 ordering in the ferrite and κ-carbide precipitation within the austenite matrix. The ultimate tensile strength increased from 1120 MPa in the annealed condition to 1230 MPa after 2 h of aging at 570 °C. Charpy V-notch toughness was evaluated at −40 °C in sub-sized specimens with a maximum in the annealed and quenched condition of 28.5 J in the L-T orientation.

Keywords: lightweight steel; age hardening; Fe-Mn-Al-C; kappa carbide; B2; NiAl

1. Introduction

Steels in the Fe-Mn-Al-C alloy system continue to be of interest as high-strength, low-density alternatives to traditional structural and automotive steels. Adding aluminum reduces the density of austenitic steels by about 1.3–1.5% per 1 wt% Al addition, while carbon is over four times more effective at reducing density [1,2]. Depending on the composition with Mn (2–30 wt%), Al (3–12 wt%), and C (up to 2 wt%), the microstructure can be ferritic, duplex, or fully austenitic with up to a 17% reduction in density when compared with quenched and tempered martensitic steels [2]. Austenitic based compositions have excellent combinations of both strength and ductility, which depends on the composition and heat treatment. Fe-Mn-Al-C steels that contain greater than 0.7 wt% C and 7 wt% Al are precipitation hardenable by the homogenous coherent precipitation of nanosized κ-carbide, $(Fe,Mn)_3AlC$, in the temperature range of 450–650 °C [2–7]. Precipitation of κ-carbide in hot rolled and recrystallized Fe-30Mn-9Al-1Si-0.9C (in wt%) steel has been shown by Bartlett et al. [8] to greatly increase strength from 950 MPa to 1160 MPa after aging for 60 h at 530 °C. However, a corresponding decrease in total elongation from 56 to 14% was also reported after aging. Additionally, cast and solution treated steels with nominal compositions in the range of Fe-30Mn-9Al-1Si-0.9C (in wt%) have shown exceptional room temperature Charpy V-notch (CVN) toughness of up to 200 J in the solution treated condition at 20 HRC. Notch toughness values up to 130 J are retained for alloys aged to a hardness of 32 HRC, however, further aging can result in a significant loss of toughness due to both intergranular and transgranular failure [8]. The loss of strain hardening and toughness during aging is the result of dislocation shearing of the κ-carbide and the corresponding glide plane softening effect and grain boundary precipitation of deleterious phases [9].

Hard intermetallic precipitates such as $D0_3$ (Fe_3Al) and B2 (FeAl) have been reported to form on austenite (γ) grain boundaries during aging, as well as through an ordering transformation within the ferrite phase of duplex steels [2,10,11]. Nickel additions of 5 wt% have been shown to promote hard B2 NiAl or (Fe,Ni)Al that is stable above the austenite recrystallization temperature, typically between 600–900 °C [2]. Controlled precipitation of B2 has the potential to significantly strengthen austenitic Fe-Mn-Al-C steels through grain refinement during controlled hot rolling, as well as precipitation of nano-sized B2 on austenite shear bands during subsequent annealing of cold rolled sheet. In a recent study by Kim et al. of a Fe-15Mn-10Al-5Ni-0.8C (wt%) steel, B2 precipitates were shown to pin austenite grain boundaries and provide excellent strength-ductility combinations of 1600 MPa, with 20% total elongation. Processing of this steel involved hot rolling at 1050 °C, followed by cold rolling with a total reduction of 67%, and concluded with annealing at 900 °C for various times. [12,13] Precipitates of B2 were identified to be 50–300 nm and were suggested to have formed on shear bands during the final annealing step.

The toughness of hot rolled lightweight Fe-Mn-Al-C steel plates has not been extensively studied. Field and Limmer [14] showed that to obtain an increase in toughness at an equivalent hardness, the grain size must be controlled and kept small to mitigate the loss of toughness during age hardening. Although κ-carbide strongly contributes to the strength of Fe-Mn-Al-C alloys, the toughness is limited due to the shearing of κ-carbide, leading to the glide plane softening effect and an associated reduction in strain hardening and toughness. The effect of Ni on the age hardening kinetics and impact toughness of hot rolled Fe-Mn-Al-C plate has not been investigated to date. The addition of nano-sized hard dislocation barriers, such as B2-type NiAl and FeAl, may result in higher combinations of strength and hardness as well as limit the glide plane softening effect. In the current study, a multiphase precipitation approach was utilized with the intention of creating an ultra-high strength hot rolled plate steel with a density reduction of at least 10% compared to traditional steels. The purpose of this work is to evaluate the microstructure–property relationships in an Fe-18Mn-10Al-0.9C-5Ni (wt%) steel thermomechanically processed to produce a fine dispersion of B2. The effect of age hardening in the temperature range of 500 to 600 °C on the microstructure and mechanical properties was evaluated.

2. Materials and Methods

A 73 kg heat with the composition of Fe-18.3Mn-10.1Al-0.9C-4.5Ni-0.0015N (wt%) was prepared in a coreless induction furnace. All compositions in the text are weight percent unless stated otherwise. The furnace charge consisted of induction iron, electrolytic manganese, aluminum, nickel pellets, and graphite. The charge was melted under argon gas cover and was calcium treated with cored calcium wire prior to removing the slag and tapping into a modified tea-pot style ladle that utilizes a ceramic dam to force molten steel from the bottom. The pouring temperature was recorded as 1540 °C, with a 140 °C superheat, during teeming into the ladle. The melt was poured into a bottom-gated phenolic no-bake silica sand Y-block mold. A 10 ppi ceramic foam filter was located in the runner. Carbon and sulfur levels were measured by combustion infrared detection analysis utilizing a LECO CS600 analyzer (LECO Corporation, St. Joseph, MI, USA). Total oxygen and nitrogen levels were measured with a LECO TC500 (LECO Corporation, St. Joseph, MI, USA). The concentrations of other elements were determined by optical emission arc spectroscopy. X-ray diffraction (XRD) was performed on a Philips X'Pert MPD (Malvern Panalytical Ltd., Malvern, UK) with a flat graphite monochromator, Ni filter, and copper K_α source.

After solidification, an 82.5 mm long × 50 mm wide × 50 mm tall rectangular bar was sectioned from the bottom of the Y-block casting directly above the chill plate. The bar was solution treated at 1150 °C for 2 h and quenched in room temperature water, and then reheated to 1050 °C for 30 min prior to hot rolling. Hot rolling was performed with a constant 1.27 mm reduction per pass. After 4 passes, the steel was returned to the furnace for reheating (5.08 mm reduction in thickness per reheat cycle). A total reduction of a 6:1 (83% reduction) to a final thickness of 8.5 mm was obtained, and a finish rolling temperature of 900 °C was recorded by an optical pyrometer. The bars were quenched into room

temperature water after finish rolling. Initial annealing was performed for 2 h at 900 °C, followed by quenching into room temperature water. A second annealing step was performed for 30 min at 950 °C, and the steel was subsequently water quenched. The hot rolled and annealed plate was sectioned and aged between 500–600 °C for up to 50 h in a salt pot furnace. A schematic of the described thermomechanical processing and subsequent heat treatment process is shown in Figure 1. Samples for microscopy were mechanically polished to a 0.05 μm finish using colloidal silica and etched with a 10% nital solution. Scanning electron microscopy (SEM) and energy dispersive spectroscopy (EDS) analysis were performed on a Hitachi S-4700 (Hitachi America, Ltd., Santa Clara, CA, USA) and Helios NanoLab 600 (Thermo Fisher Scientific, Waltham, MA, USA). Sub-sized tensile specimens with 6 mm × 6 mm cross section and 25 mm gauge length were prepared parallel to the rolling direction in the 950 °C annealed and aged conditions and tested at room temperature as per ASTM E8 guidelines. Charpy V-notch toughness was determined using 10 mm × 7.5 mm × 55 mm (3/4 sub-size) bars at −40 °C in accordance with ASTM E23 in both the T-L and L-T orientations.

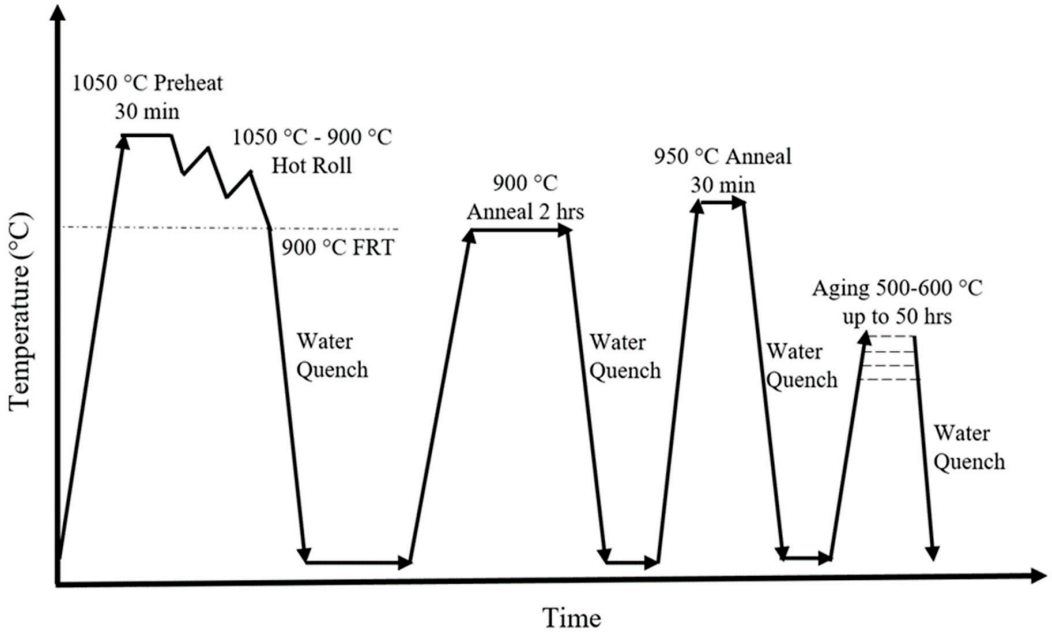

Figure 1. Schematic diagram of thermomechanical processing and subsequent heat treatment for the Fe-18Mn-10Al-0.9C-5Ni steel.

3. Results

The as-cast microstructure obtained near the chill plate in Figure 2a is shown to consist of primary δ-ferrite at the center of austenite dendrites. Dark etching regions corresponding to interdendritic regions contained significant precipitation as a result of alloy segregation. The as-rolled and quenched microstructure is shown in Figure 2b consisting of δ-ferrite stringers elongated during deformation of the primary δ-ferrite. Globular B2 precipitates formed within the matrix and on austenite grain boundaries are also observed in the rolled microstructure.

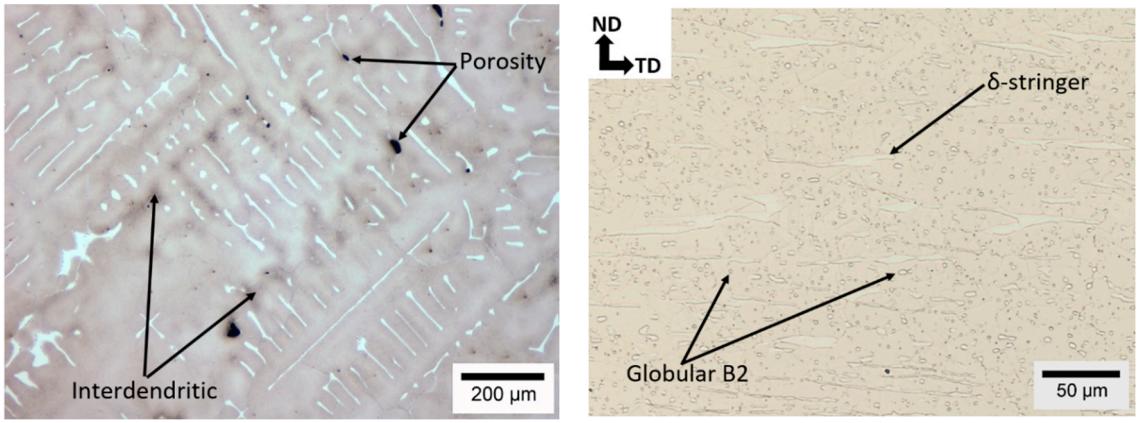

(**a**) (**b**)

Figure 2. Optical micrographs of Fe-18Mn-10Al-0.9C-5Ni steel in the (**a**) as-cast condition and (**b**) after hot rolling at 1050 °C.

An optical micrograph of the steel after annealing for 2 h at 900 °C is shown in Figure 3a. Dense regions of sub-micron sized B2 precipitation are formed within austenite grains. In some cases, B2 platelets are observed to precipitate and coarsen along the entire length of shear bands as indicated within Figure 3a. A corresponding secondary electron image in Figure 3b shows a light contrast phase that has a morphology consistent with coarse grained κ-carbide precipitation 2–3 microns in size located on γ-δ interfaces as well as on δ-ferrite grain boundaries, while fine B2 platelets on the order of 250 nm in thickness were observed to have precipitated within the austenite. Due to the undesirable coarse grained κ-carbide, a subsequent 30 min anneal at 950 °C followed by water quenching was performed to dissolve grain boundary κ-carbide. The resulting microstructure is shown in Figure 4a,b, with no coarse κ-carbide observed. Globular B2, however, was still observed on γ-γ grain boundaries. These globular particles are assumed to have been formed from the coarsening of the B2 plates that were observed before the second annealing step.

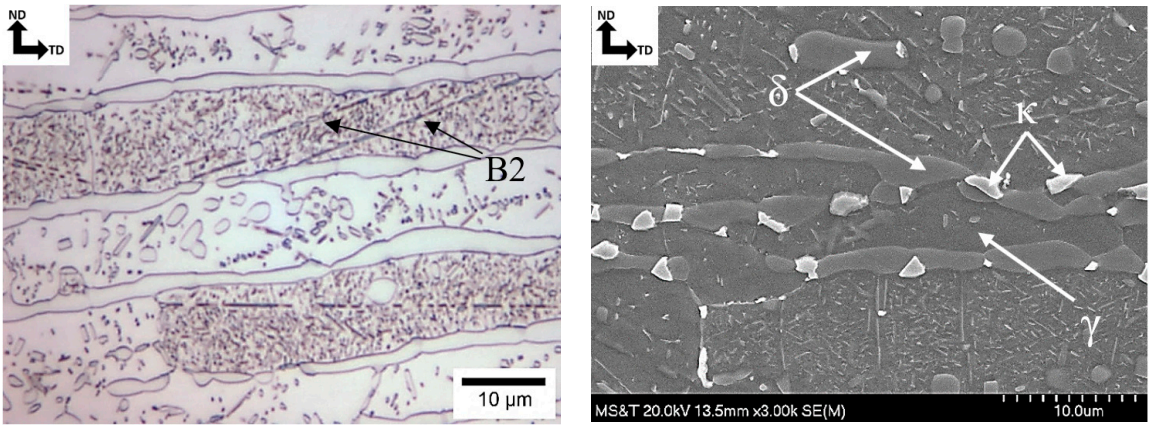

(**a**) (**b**)

Figure 3. (**a**) Optical micrograph and (**b**) secondary electron image of the hot rolled steel annealed at 900 °C for 2 h.

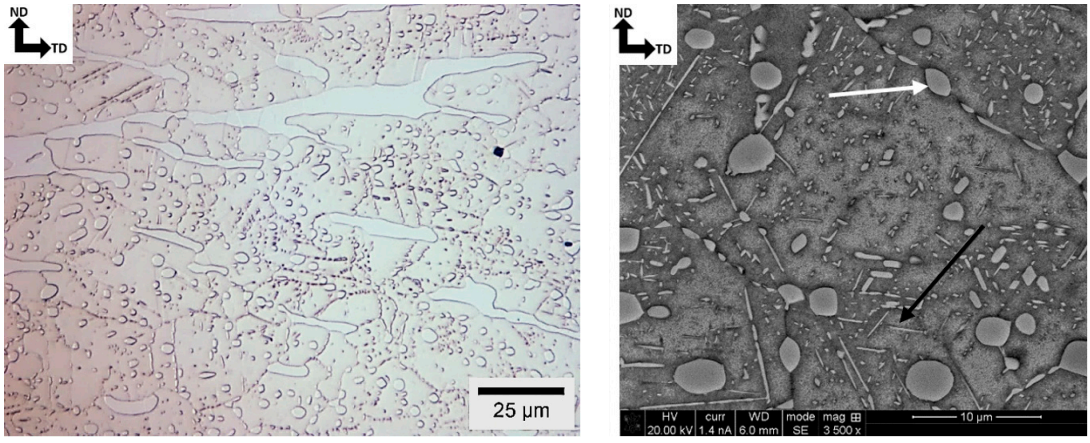

(**a**) (**b**)

Figure 4. (**a**) Optical image of Fe-18Mn-10Al-0.9C-5Ni specimen after secondary annealing at 950 °C for 30 min. (**b**) Secondary electron image shows globular B2 on grain boundaries (white arrow) and platelets of matrix B2 that are coarsening in crystallographic directions (black arrow).

Optical micrographs in Figure 5a,b show the microstructures after aging for 1 h and 50 h at 530 °C. Extended aging times and higher temperatures produced a lamellar eutectoid decomposition ($\gamma \rightarrow \kappa + \alpha$) at γ-γ grain boundaries and at γ-B2 interfaces, as shown in Figure 5b. Grain boundary κ-carbide is expected to have a deleterious effect on ductility and toughness, as noted previously, and should therefore be minimized.

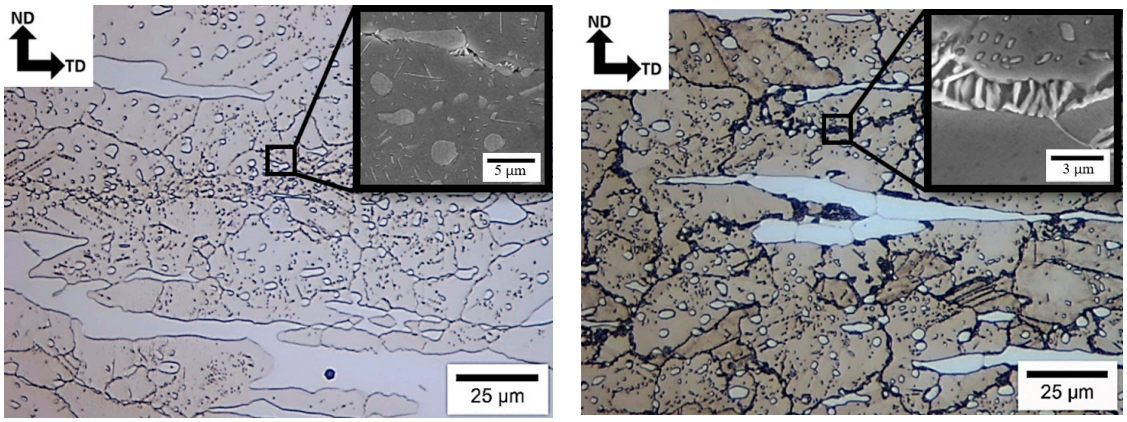

(**a**) (**b**)

Figure 5. Optical micrographs and corresponding higher magnification secondary electron images of the Fe-18Mn-10Al-0.9C-5Ni alloy in the annealed condition and aged at 530 °C for (**a**) 1 h and (**b**) 50 h. Precipitation of ferrite and lamellar κ-carbide on austenite grain boundaries was observed at 50 h at 530 °C.

EDS results of the regions shown in Figures 3 and 4 are presented in Table 1. From the EDS compositional analysis, the coarse particles in Figure 3 are shown to be rich in C and Al, consistent with κ-carbide. It should be noted that carbon is a light element, and quantitative assessment utilizing EDS is not possible, however, qualitative values can be extracted from the spectra. Aluminum and nickel are shown to partition to the ferrite and B2 phases. No significant change in chemistry was observed in the austenite and B2 phases after the additional 950 °C anneal for 30 min compared to the 900 °C anneal. The compositions of the different phases after age hardening for 17 h at 600 °C is shown in Table 1. After aging, the aluminum content in the austenite decreased, while the carbon content greatly increased. The lamellar κ-carbide phase exhibited enrichment in Mn, Al, and C, compared to

the austenite phase. EDS analysis showed that the compositions of the δ-ferrite stringers and B2 were largely unchanged after aging.

Table 1. Chemistries of phases in the wrought plate after various stages of processing from energy dispersive spectroscopy (EDS) analysis.

Heat Treatment	Phase	Composition in wt%				
		Fe	Mn	Al	C	Ni
Annealed 2 h @ 900 °C	**γ-austenite**	67.1	18.2	9.5	1.7	3.5
	κ-carbide	64.0	18.6	12.1	2.5	2.8
	δ-stringer	63.2	11.7	14.4	-	9.9
	B2	61.4	11.9	15.2	-	10.5
Annealed 2 h @ 900 °C 0.5 h @ 950 °C	**γ-austenite**	67.1	18.6	8.9	1.8	3.8
	δ-stringer	60.8	11.3	13.9	-	11.1
	B2	60.8	12.0	14.1	-	11.1
Annealed 2 h @ 900 °C 0.5 h @ 950 °C aged @ 600 °C for 17 h	**γ-austenite**	65.6	18.2	8.5	4.4	3.3
	κ-carbide	61.6	19.4	10.0	6.1	2.9
	δ-stringer	63.1	11.9	14.4	-	10.6
	B2	61.1	13.1	13.6	-	10.2

XRD patterns are shown in Figure 6 for specimens aged 1, 8, and 50 h at 530 °C. The measured weight percent of ferrite and austenite, excluding κ-carbide, are shown in Table 2. There was no evidence of differentiation between ferrite and B2 ordering in the diffraction patterns in this study. The amount of ferrite/B2 was determined using Rietveld refinement and was found to increase with aging time from 17% to 25%. κ-carbide was observed in the XRD pattern only after 50 h of aging, as shown in Figure 6b, however, it could not be accurately quantified. The (111) austenite peak at 42.5° shows development of characteristic spinodal decomposition to form side-bands. The side-band at 42.2° is due to lattice parameter dilation associated with carbon ordering in solute rich austenite to form homogeneous κ-carbide precipitation. The side-band at 43.0° is due to lattice parameter contraction of the solute lean austenite zones remaining after homogeneous κ-carbide precipitation and the loss of Al from the matrix. One small tungsten peak was present at 41.5° as the result of an aging X-ray tube.

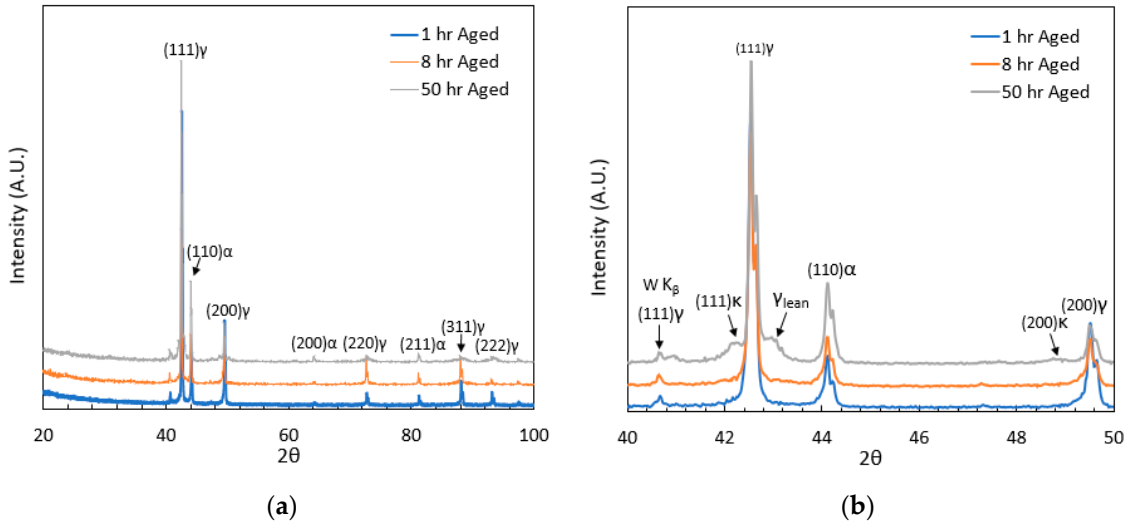

Figure 6. (**a**) X-ray diffraction (XRD) patterns from for the 1, 8, and 50 h aged at 530 °C specimen. (**b**) Truncated XRD spectra for the 1, 8, and 50 h aged at 530 °C specimen.

Table 2. Weight percent of austenite and ferrite/B2 as a function of aging time as determined by XRD using Rietveld refinement assuming a duplex microstructure of only ferrite/B2 and austenite.

Aging Time at 530 °C	Austenite %	Ferrite/B2 %
1 h	82.7	17.3
8 h	83.8	16.2
50 h	75.3	24.7

Age hardening curves for specimens aged in the temperature range of 500–600 °C are shown in Figure 7a. The hardness increases rapidly during aging, from 32 HRC to 37 HRC at 500 °C and 42 HRC at 600 °C after 0.25 h of aging. The results exhibit typical precipitation hardening kinetics in which hardening rate increases with increasing temperature. For 530–600 °C, the peak hardness decreases with increasing temperature. Vicker's microhardness measurements within both the austenite and primary δ-ferrite stringers were conducted as a function of aging at 500 °C for up to 8 h, as shown in Figure 7b. The results show that both ferrite and austenite increase in hardness during aging. However, the hardness of the ferrite appears to increase at a faster rate. The aging treatment of 570 °C for 2 h resulted in a hardness of 44 ± 0.5 HRC with minimal grain boundary precipitation, and this aging condition was further explored for comparison of mechanical properties.

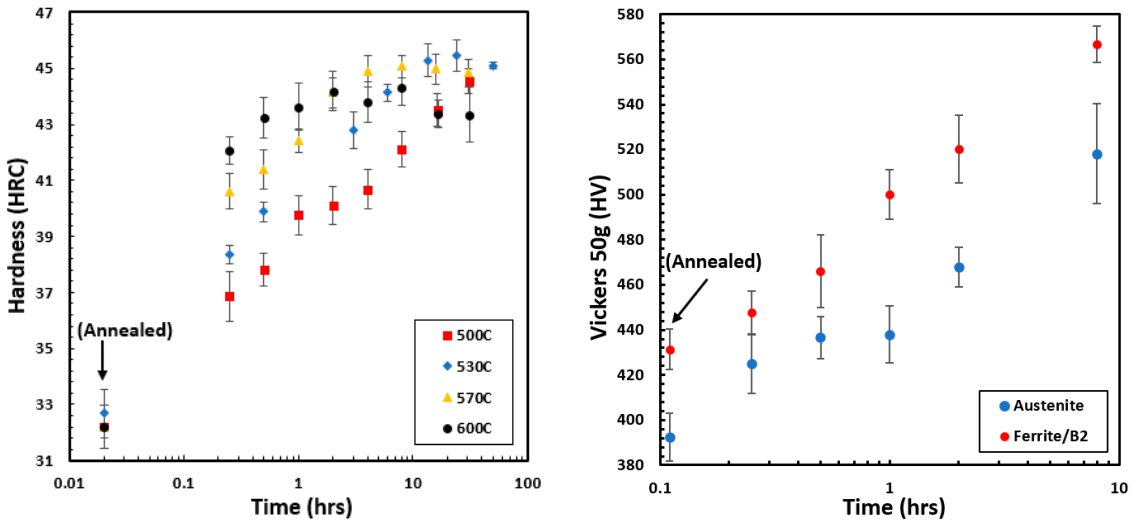

Figure 7. (**a**) Hardness as a function of aging time for the Fe-18Mn-10Al-0.9C-5Ni alloy. (**b**) Vickers microhardness (with a 50 g load) of ferrite/B2 stringers and austenite after aging at 500 °C. The first data point for each phase is the 950 °C annealed condition.

Tensile properties are reported in Table 3. Results are the average of three specimens per condition with a 68% CI. The annealed and quenched tensile specimens had an ultimate tensile strength (UTS) of 1120 MPa and a total elongation (TE) of 26.4%. The reduction in area (RA) in the annealed condition was determined to be 23.6%. After aging for 2 h at 570 °C, the yield strength increased from 810 to 1150 MPa (42% increase) while the ultimate tensile strength only increased from 1120 to 1230 MPa (10% increase). However, aging sharply reduced the TE from 26.4 to 12.1% (54% decrease), and the RA was reduced to 13.3% (44% decrease).

Table 3. Room temperature tensile properties of the Fe-18Mn-10Al-0.9C-5Ni steel as a function of heat treatment.

Heat Treatment	Yield Strength (MPa)	UTS (MPa)	% Total Elongation	% Reduction of Area
Annealed and quenched	810 ± 42	1120 ± 128	26 ± 15	24 ± 12
Aged hardened at 570 °C for 2 h	1150 ± 93	1230 ± 102	12 ± 7	13 ± 8

The Charpy V-notch (CVN) toughness at −40 °C in the annealed and quenched condition and for the steel aged for 2 h at 570 °C is given in Table 4. It is shown that the alloy exhibits significant anisotropy for both tested conditions. The CVN toughness is reduced nearly 75% when the crack path is oriented parallel to the δ-ferrite stringers in the T-L orientation. After aging, the anisotropy is negligible, and the material now behaves in a brittle fashion with an absorbed energy of only 2 joules.

Table 4. Charpy V-notch impact toughness for 3/4 subsize specimens tested at −40 °C in the annealed and aged condition.

Orientation	Annealed [J]	Annealed and Aged at 570 °C 2 h [J]
L-T	28.5 ± 2.7	2.3
T-L	7.3 ± 0.2	2.0

Optical micrographs in Figure 8a show the polished longitudinal sections of tested tensile bars in the annealed condition and reveal that the ferrite stringers fracture in a brittle manner during deformation. Ferrite stringers on the corners of tensile specimens were determined to be the source of premature failure before the onset of necking. An alloy system with similar Ni and Al levels treated above 900 °C reported forming B2 precipitates in the ferrite rather than full transformation of the ferrite to B2 [13]. Therefore, this brittle behavior was not anticipated, and it is theorized that the ferrite may have at least partially transformed to B2-FeAl and/or B2-NiAl during cooling from hot rolling and annealing temperatures. This is supported by the observed partitioning of Ni, a traditional austenite stabilizer, to ferrite/B2 shown in Table 1. Cleavage fracture facets perpendicular to the main fracture plane were associated with the brittle fracture of ferrite/B2 as shown in Figure 8b. The austenitic matrix exhibits microvoid coalescence around hard B2 precipitates. An optical micrograph of the aged alloy within the tensile fracture area is presented in Figure 9a. It should be noted that aging for 2 h at 570 °C produced minimal grain boundary precipitation of κ-carbide on γ-γ and γ-α/B2 grain boundaries. Fracture was mainly intergranular with delamination of the ferrite/B2 stringers from the austenite matrix. Cleavage fracture was also observed in the ferrite/B2 stringers. The SEM image in Figure 9b shows the tensile fracture surface of the aged specimen. A mixed mode fracture is shown in Figure 9b with both intergranular fracture along grain boundaries as well as some areas of microvoid nucleation and coalescence around B2 particles.

The fracture surfaces of the annealed notched impact toughness specimens that were tested at −40 °C are shown in Figure 10a,b. Ductile fracture is observed in the austenite matrix, and cleavage fracture is noted within ferrite/B2 stringers. Similar to reinforced composites, toughness in the T-L direction is drastically reduced, with brittle crack propagation along the length of the ferrite/B2 stringers, as shown in Figure 10b. The fracture surfaces of the aged L-T Charpy specimens are shown in Figure 11a,b for a specimen that was annealed and aged for 2 h at 570 °C. The aged specimens showed mainly brittle behavior and display both intergranular fracture along grain boundaries and transgranular cleavage fracture through ferrite/B2.

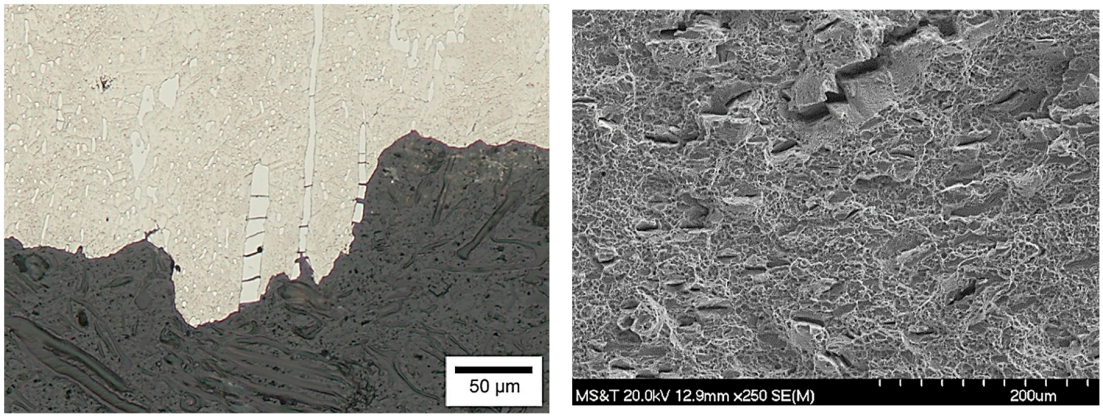

(**a**) (**b**)

Figure 8. (**a**) Optical micrograph of the 950 °C annealed tensile specimen sectioned perpendicular to the fracture surface and parallel to the tensile loading direction. (**b**) Secondary electron image of tensile fracture surface in the annealed condition.

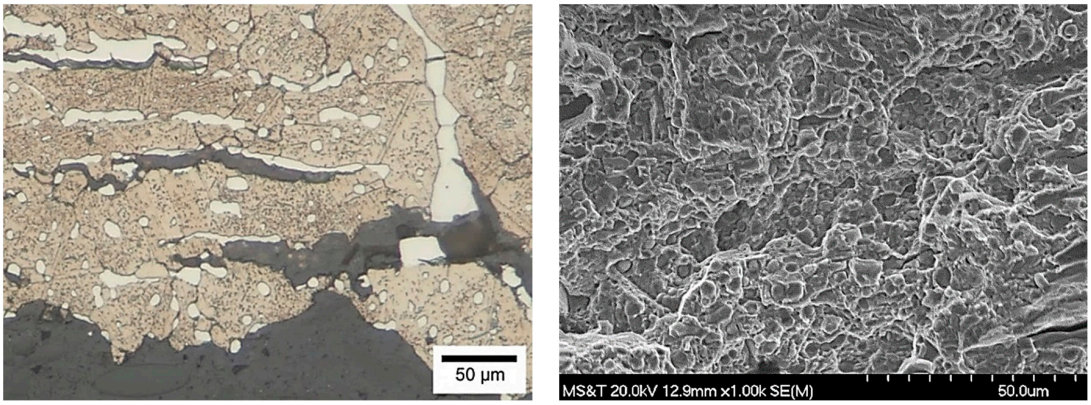

(**a**) (**b**)

Figure 9. (**a**) Optical micrograph of the annealed and aged for 2 h at 570 °C tensile specimen sectioned perpendicular to the fracture surface and parallel to the tensile loading direction. (**b**) The secondary electron image of the tensile fracture surface in the aged condition.

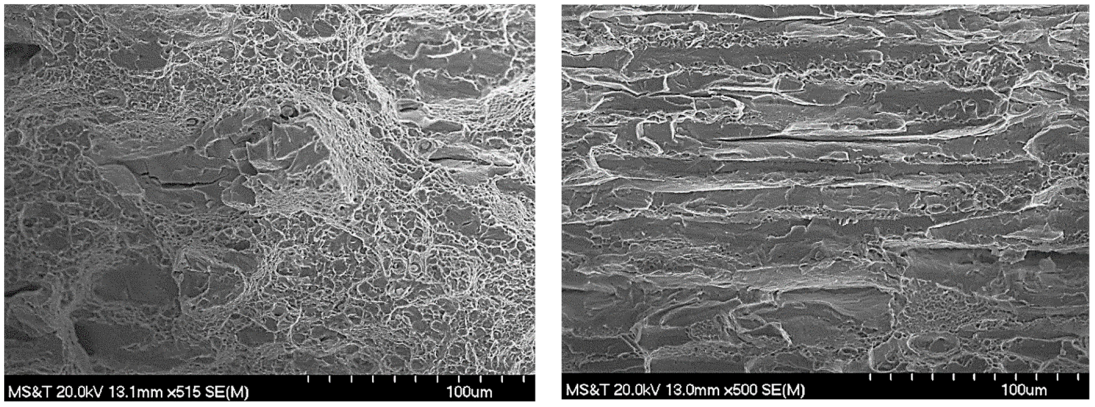

(**a**) (**b**)

Figure 10. Secondary electron images of the fracture surface of an annealed specimen broken at −40 °C in the (**a**) L-T and (**b**) T-L orientations.

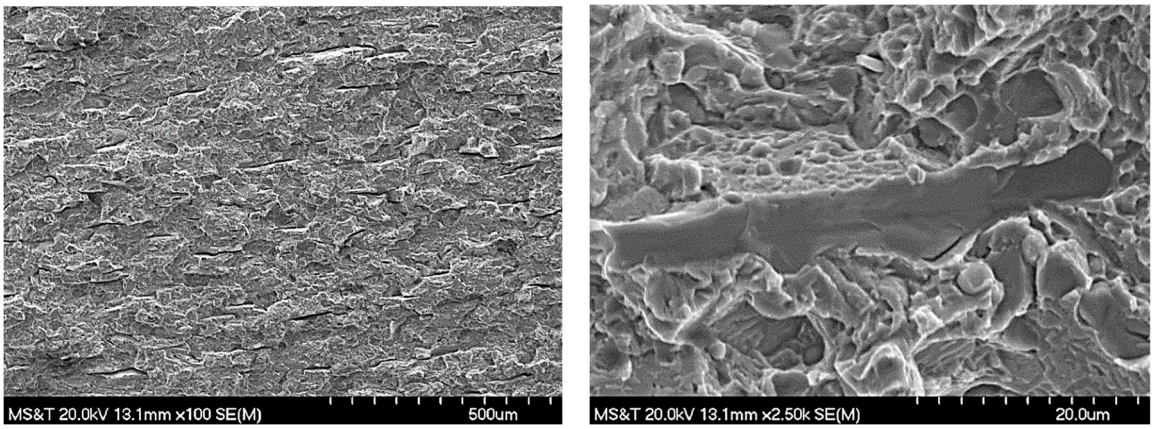

(**a**) (**b**)

Figure 11. (**a**,**b**) Secondary electron images of the CVN fracture surface of the specimen that was annealed and aged for 2 h at 570 °C and broken in the L-T orientation at −40 °C.

4. Discussion

The as-hot rolled microstructure of the Fe-18Mn-10Al-0.9C-5Ni steel consisted of an austenitic matrix with primary ferrite stringers that may have partially or fully transformed to B2 after rolling and globular B2 precipitation on recrystallized austenite grain boundaries and annealing twins (Figure 2). After initial annealing at 900 °C, fine B2 platelets were observed that were coarsened upon subsequent annealing at 950 °C (Figures 3 and 4). This range of B2/ferrite morphology is in good agreement with Kim et al. [12], who observed three different morphologies of (Fe,Ni)Al type B2, although the B2 formed within this study was significantly coarser than the nano-scaled particles observed in the work by Kim et al. because the high dislocation density obtained through cold working of sheet product was not possible with thick plate. The nanoscale B2 (Fe,Ni)Al precipitation on the dislocation networks was instead observed as coarsened plates after annealing in this study.

The stringers in the 950 °C annealed steel are brittle and exhibit cleavage fracture at room temperature during quasi-static tensile deformation (Figure 8). In contrast, Rahnama et al. [13,15] reported greater ductility in a similar alloy after annealing at 900 °C when the stringers were comprised of disordered ferrite with nano-sized B2 precipitates. The B2 precipitates appeared as a uniform distribution of rounded or disc shaped <200 nm ordered domains with a cube-on-cube relationship with ferrite [13]. This suggests that there is a larger degree of ordering in the stringers in the present study, due in part to the subsequent annealing at 950 °C. Annealing of the present alloy only at 900 °C resulted in the formation of a deleterious coarse grained κ-carbide, hypothesized to be stabilized by the higher Mn and C content.

The precipitation of equiaxed B2 on austenite grain boundaries and within austenite grains in the as-hot rolled and annealed specimens (Figures 3 and 4) is consistent with the morphology and size reported in previous studies with similar processing [12,13]. Nano-sized precipitation of B2 within austenite grains enhances strength, however, coarse B2 on austenite grain boundaries and preferential crack nucleation along γ-B2 interfaces have been shown to significantly reduce ductility [13,16].

B2 precipitation on dislocations or on shear bands within the austenite results in a fine distribution of nano-sized (50–300 nm) particles that greatly strengthen the matrix while minimizing degradation of ductility. However, after subsequent annealing at 950 °C, the B2 in the austenite matrix coarsened substantially into long plates that were as much as 10 microns in size (Figure 4). Coarsening of elongated B2 from transmission electron microscopy and atom probe tomography analyses have been reported to be the result of fast pipe diffusion of Ni and Al along dislocations [15]. Balluffi reported that diffusion of substitutional elements like Ni and Al through dislocation cores is typically 40 to 70% of the activation energy required for bulk diffusion [17]. Kim et al. showed that B2 precipitates under

80 nm in diameter behave as hard Orowan barriers that are not sheared but looped by dislocations [12]. Coarsening of the B2 precipitates should be carefully controlled during heat treatment because it is well known that Orowan strengthening is inversely proportional to the spacing of the particles.

Ni and Al were shown to partition to the ferrite/B2 phases with no significant differences measured for changes in morphology or annealing temperature (Table 1). Ni and Al were enriched from bulk composition of 4.5 and 10.1 wt% to 10–11 and 14–15 wt% in the ferrite/B2, respectively. For globular B2, the Ni enrichment values are consistent with those reported by Rahnama et al. [13] after a 900 °C anneal as shown in Table 5. The lower Al enrichment levels observed in this study may be related to the increased Mn and C of the bulk composition and the effect on Al solubility in the ferrite/B2. Interestingly, Rahnama et al. reported that increasing the annealing temperature increased the partitioning of Ni and Al into the B2. Although the annealing times were not provided, this may suggest that the times used in this study were shorter, resulting in less enrichment of the ferrite/B2. The Ni and Al enrichment reported by Rahnama in the stringer was also significantly higher for isothermal holds of a comparable temperature.

Table 5. Comparison of the B2 composition from this work to the reported work of Rahnama, data from [13].

Study	Condition	Phase	Ni (wt%)	Al (wt%)
Present	all conditions	all ferrite/B2	10–11	14–15
REF [13]	900 °C anneal	globular B2 in γ	9.7 [10.1]	17.1 [18.7]
	[1050 °C anneal]	ferrite/B2 stringer	15.1 [19.2]	20.4 [21.3]

Age hardening between 500–600 °C produced a significant hardening effect (Figure 7a) accompanied by a range of observed microstructural modifications: Coarsening of B2, grain boundary eutectoid decomposition of the austenite to lamellar κ-carbide and ferrite, and precipitation of κ-carbide. The hardening was shown to occur in both the ferrite/B2 and austenite phases (Figure 7b). The hardening observed in the ferrite/B2 is attributed to the B2 ordering reaction, which has been shown to greatly increase the hardness of the ferrite matrix [18]. Further, the partitioning of Ni to the B2 has been suggested to lead to an increase in B2 hardness because of the greater bond strength between Ni-Al compared to that of Fe-Al in the B2 structure [13]. The degree of hardening observed in the ferrite/B2 is consistent with the hardness of ferrite/B2 reported for another B2-NiAl strengthened alloy aged at similar conditions [19]. The austenite hardening is presumed to be due to κ-carbide formation, as qualitatively shown with XRD (Figure 6) and by the appropriate composition space for κ-carbide formation at these temperatures measured by EDS (Table 1).

The annealed and quenched condition showed a good combination of strength and ductility with an average ultimate tensile strength (UTS) of 1120 MPa and an average total elongation of 26% (Table 3). This can be compared with a Fe-15Mn-10Al-0.8C-5Ni steel hot rolled with a UTS of 1335 MPa and 10% elongation, which was annealed at 900 °C [13]. During tensile deformation of the annealed specimens, B2 stringers were observed to fracture, while austenite accommodates the tensile strain without fracturing and remains quite ductile, as seen in Figure 8a,b. Fractography of the annealed tensile specimen fracture surface in Figure 8b revealed that these stringers were the initial source of failure. These observations are in agreement with fractography performed on duplex Ni-25Al-xFe alloys tensile specimens that reported cleavage fracture of the B2 dendrites and γ-B2 interfaces ruptured and were the primary crack propagation path [16]. This early failure is also the source of the wide standard deviation in reported mechanical properties in Table 3. The current steel has about 200 MPa less strength and more than twice the ductility, as previously reported in a hot rolled steel in Rahnama's study. The differences in mechanical properties are suggested to be due to a combination of effects including the amount of austenite present, degree of ordering in the ferrite after annealing, and possible variations in annealing time that results in over-coarsening matrix NiAl precipitates. Recent studies have shown that increasing the annealing time from 2 to 15 min at 900 °C

produced almost a 200 MPa drop in UTS in cold rolled and annealed sheet steels with a corresponding 10% increase in ductility [20]. Therefore, annealing times should be minimized to prevent coarsening of B2 that results in reduced strength.

The aged tensile specimens in the current study achieved higher strengths with an average UTS of 1230 MPa, while total elongation was lowered to an average of only 12%. The increase in strength and decrease in elongation with aging is likely the result of B2 ordering within stringers and nano-sized κ-carbide precipitation within the austenite matrix. The micrographs in Figure 9a,b of the aged tensile specimen reveal that the fracture mode changes to intergranular where fracture now occurs along austenite grain boundaries, as well as in areas with κ-carbide precipitation at the interface between austenite and B2. Fractography of the aged tensile fracture surface in Figure 9b reveals that large B2 stringers remain the source of premature failure.

Figure 12 shows the tensile properties of the current steel in comparison to similar composition steels with 5% Ni and a fully austenitic hot rolled Fe-30Mn-9Al-1Si-0.9C-0.5Mo steel with a similar grain size. The results show that the current steel has higher combinations of strength and ductility when compared to the Fe-30Mn-9Al-1Si-0.9C-0.5Mo steel and similar 5% Ni alloys annealed below 700 °C.

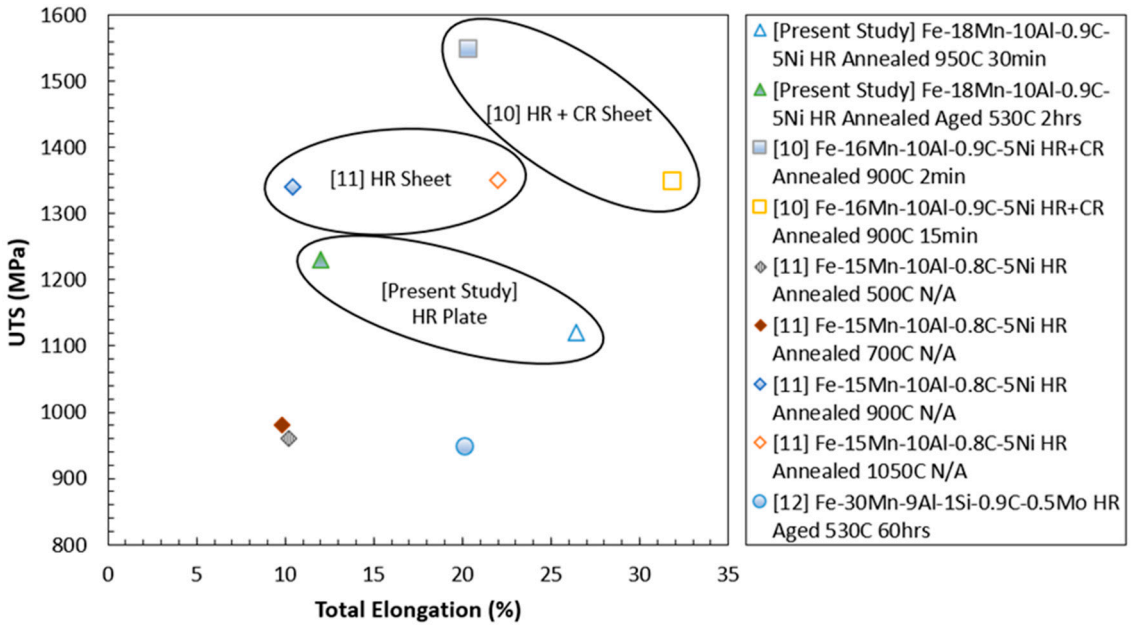

Figure 12. Ultimate tensile strength (UTS) as a function of total elongation (%) for various wrought hot rolled (HR) and cold rolled (CR) Fe-Mn-Al-C steels and annealing heat treatments.

The Charpy V-notch toughness of this steel was highly dependent on heat treatment and sample orientation with the rolling direction, with the presence of the brittle B2 stringers having a significantly deleterious effect on notch toughness (Table 4). The annealed condition had the highest toughness of 28.5 J in the L-T direction with crack propagation perpendicular to B2 stringers. Once fracture occurs along the stringers in the T-L direction, notch toughness drastically reduces to less than 8 J. After aging at 570 °C for 2 h, notch toughness is significantly reduced in both the L-T and T-L direction to an average of 2 J. Fractography of the annealed specimens (Figure 10) reveals ductile fracture in the austenite with brittle fracture across the ferrite stringers in the L-T orientation. However, the L-T fracture surface in the annealed condition was notably different (Figure 10b) due to fracture along the ferrite stringers that caused a severe drop in notch toughness for this orientation. Fractography of the Charpy specimens in the aged condition (Figure 11) continued to show brittle cleavage of the B2 now accompanied by less ductile austenite. The significant loss of ductility in the aged condition is consistent with precipitation of κ-carbide on grain boundaries and promoting intergranular fracture.

These results show that brittle B2 stringers should be eliminated as much as possible for maximum toughness and ductility and to provide less anisotropy in the rolled structure. Increasing the amount of Mn and C while slightly reducing the amount of Al may be one strategy to eliminate primary ferrite stringers. Shorter annealing times at 950 °C should be utilized to prevent over-coarsening of B2 along shear bands and on grain boundaries. In addition, heat treatments or an alloying approach to reduce the amount of κ-carbide precipitation on grain boundaries may be effective at increasing the toughness of this steel after aging.

5. Conclusions

This study investigated the role of thermomechanical processing and heat treatment on the microstructural development and mechanical properties of a Fe-18Mn-10Al-0.9C-5Ni steel that was hot rolled, annealed, and aged for plate applications. Annealing time and temperature are a critical factor in mechanical property optimization in this alloy system. Annealing below the eutectoid decomposition temperature produced undesirable coarse κ-carbide on both ferrite-ferrite boundaries and ferrite-austenite interfaces. Shorter annealing times should be utilized at 950 °C to prevent coarsening of the B2 precipitates into platelets along grain boundaries and shear bands. Isothermal heat treatment of this alloy between 500–600 °C increased the hardness through the precipitation of κ-carbide and ordering of the ferrite to B2, as observed by the increase in hardness of both phases during aging. After annealing and aging, this alloy achieved a hardness of 45 HRC with a 1200 MPa ultimate tensile strength. Brittle ferrite/B2 stringers result in premature failure of tensile specimens prior to necking in both the annealed and aged conditions, and austenite decomposition ultimately limits the ductility and impact toughness in the aged condition. The ferrite/B2 stringers induce strong anisotropy in the impact properties leading to a 75% reduction of the notch toughness when the fracture path is parallel to the stringers.

Author Contributions: M.P. performed the methodology, characterization, analysis, and original draft preparation. L.B., D.M.F., and K.R.L. assisted with analysis, supervision, writing, review, and editing of the draft. All authors have read and agreed to the published version of the manuscript.

Funding: This research was sponsored in part by the DLA—Troop Support, Philadelphia, PA and the Defense Logistics Agency Logistics Operations, J68, Research & Development, Ft. Belvoir, VA under a subcontract from Steel Founders' Society of America, contract number SP4701-17-D-1161. Funding for this project was also received from the Army Research Office under contract number W911NF-19-2-0044.

Acknowledgments: Special thanks to Eric Bohannan for his assistance with the XRD analysis, and to the undergraduate researcher, Ryan Van Dyke, for his assistance with material preparation.

Conflicts of Interest: The authors declare no conflict of interest.

References

1. Kim, H.; Suh, D.-W.; Kim, N.J. Fe-Al-Mn-C Lightweight Structural Alloys: A Review on the Microstructures and Mechanical Properties. *Sci. Technol. Adv. Mater.* **2013**, *14*, 014205. [CrossRef] [PubMed]
2. Chen, S.; Rana, R.; Haldar, A.; Ray, R.K. Current State of Fe-Mn-Al-C Low Density Steels. *Prog. Mater. Sci.* **2017**, *89*, 345–391. [CrossRef]
3. Witkowska, M.; Zielińska-Lipiec, A.; Kowalska, J.; Ratuszek, W. Microstructural Changes in a High-Manganese Austenitic Fe-Mn-Al-C Steel. *Arch. Metall. Mater.* **2014**, *59*, 971–975. [CrossRef]
4. Cheng, W.C.; Cheng, C.Y.; Hsu, C.W.; Laughlin, D.E. Phase Transformation of the L12 Phase to Kappa-Carbide After Spinodal Decomposition and Ordering in an Fe–C–Mn–Al Austenitic Steel. *Mater. Sci. Eng. A* **2015**, *642*, 128–135. [CrossRef]
5. Li, M.C.; Chang, H.; Kao, P.W.; Gan, D. The effect of Mn and Al contents on the solvus of κ phase in austenitic Fe-Mn-Al-C alloys. *Mater. Chem. Phys.* **1999**, *59*, 96–99. [CrossRef]
6. Acselrad, O.; Kalashnikov, I.S.; Silva, E.M.; Khadyev, M.S.; Simao, R.A. Diagram of Phase Transformations in the Austenite of Hardened Alloy Fe-28% Mn-8.5% Al-1% C-1.25% Si as a Result of Aging due to Isothermal Heating. *Met. Sci. Heat Treat.* **2006**, *48*, 543–553. [CrossRef]

7. Cheng, W.C.; Song, Y.S.; Lin, Y.S.; Chen, K.F.; Pistorius, P.C. On the eutectoid reaction in a quaternary Fe-C-Mn-Al alloy: Austenite → ferrite + kappa-carbide + M23C6 carbide. *Metall. Mater. Trans. A* **2014**, *45*, 1199–1216. [CrossRef]
8. Bartlett, L.N.; van Aken, D.C. High Manganese and Aluminum Steels for the Military and Transportation Industry. *JOM* **2014**, *66*, 1770–1784. [CrossRef]
9. Acselrad, O.; Pereira, L.C.; Dille, J.; Delplancke, J.L. Room-Temperature Cleavage Fracture of FeMnAlC Steels. *Metall. Mater. Trans. A* **2004**, *35*, 3863–3866. [CrossRef]
10. Etienne, A.; Massardier-Jourdan, V.; Cazottes, S.; Garat, X.; Soler, M.; Zuazo, I.; Kleber, X. Ferrite Effects in Fe-Mn-Al-C Triplex Steels. *Metall. Mater. Trans. A* **2014**, *45*, 324–334. [CrossRef]
11. Kubaschewski, O. *Iron—Binary Phase Diagrams*, 1st ed.; Springer: Berlin, Germany, 1982.
12. Kim, S.-H.; Kim, H.; Kim, N.J. Brittle Intermetallic Compound Makes Ultrastrong Low-Density Steel with Large Ductility. *Nature* **2015**, *518*, 77–79. [CrossRef] [PubMed]
13. Rahnama, A.; Kotadia, H.; Sridhar, S. Effect of Ni Alloying on the Microstructural Evolution and Mechanical Properties of Two Duplex Light-Weight Steels during Different Annealing Temperatures: Experiment and Phase-Field Simulation. *Acta Mater.* **2017**, *132*, 627–643. [CrossRef]
14. Field, D.M.; Limmer, K.R. Effect of Solution Treatment on Grain Size and Toughness of Lightweight Fe-Mn-Al-C Steel. In Proceedings of the 2019 AISTech Conference Proceedings, Pittsburgh, PA, USA, 6–9 May 2019. [CrossRef]
15. Jiang, S.; Wang, H.; Wu, Y.; Liu, X.; Chen, H.; Yao, M.; Gault, B.; Ponge, D.; Raabe, D.; Hirata, A.; et al. Ultrastrong steel via minimal lattice misfit and high density nanoprecipitation. *Nature* **2017**, *544*, 460–464. [CrossRef] [PubMed]
16. Tsau, C.-H. The Effects of Interfaces on the Mechanical Properties of Ni–Al–Fe Intermetallics. *Mater. Chem. Phys.* **2002**, *75*, 296–300. [CrossRef]
17. Balluffi, R.W. On measurements of self-diffusion rates along dislocations in FCC Metals. *Phys. Status Solidi* **1970**, *41*, 11–21. [CrossRef]
18. Cayetano, N.; Saucedo, M.; Donrantes, H.; Gonzalex, J.; Villegas, J.; Lopez, V. Ostwald ripening process of coherent β′ precipitates during aging in Fe-Ni-Al and Fe-Ni-Al-Cr alloys. *Adv. Mater. Sci. Eng.* **2014**, *2015*, 485626.
19. Jiao, Z.B.; Luan, J.H.; Miller, M.K.; Liu, C.T. Precipitation mechanism and mechanical properties of an ultra-high strength steel hardened by nanoscale NiAl and Cu particles. *Acta Mater.* **2015**, *97*, 58–67. [CrossRef]
20. Kim, H. Strain hardening of novel high Al low density steel consisting of austenite matrix and B2-ordered intermetallic second phase in the perspective on non cell forming face centered cubic alloy with high stacking fault energy. *Scr. Mater.* **2019**, *160*, 29–32. [CrossRef]